A Revised Tropical Cyclone Rapid Intensification Index for the Atlantic and Eastern North Pacific Basins

JOHN KAPLAN

NOAA/AOML/Hurricane Research Division, Miami, Florida

MARK DEMARIA AND JOHN A. KNAFF

NOAA/NESDIS/Regional and Mesoscale Meteorology Team, Fort Collins, Colorado

(Manuscript received 27 February 2009, in final form 22 June 2009)

ABSTRACT

A revised rapid intensity index (RII) is developed for the Atlantic and eastern North Pacific basins. The RII uses large-scale predictors from the Statistical Hurricane Intensity Prediction Scheme (SHIPS) to estimate the probability of rapid intensification (RI) over the succeeding 24 h utilizing linear discriminant analysis. Separate versions of the RII are developed for the 25-, 30-, and 35-kt RI thresholds, which represent the 90th (88th), 94th (92nd), and 97th (94th) percentiles of 24-h overwater intensity changes of tropical and subtropical cyclones in the Atlantic (eastern North Pacific) basins from 1989 to 2006, respectively. The revised RII became operational at the NHC prior to the 2008 hurricane season.

The relative importance of the individual RI predictors is shown to differ between the two basins. Specifically, the previous 12-h intensity change, upper-level divergence, and vertical shear have the highest weights for the Atlantic basin, while the previous 12-h intensity change, symmetry of inner-core convection, and the difference in a system's current and maximum potential intensity are weighted highest in the eastern North Pacific basin.

A verification of independent forecasts from the 2006 and 2007 hurricane seasons shows that the probabilistic RII forecasts are generally skillful in both basins when compared to climatology. Moreover, when employed in a deterministic manner, the RII forecasts were superior to all other available operational intensity guidance in terms of the probability of detection (POD) and false alarm ratio (FAR). Specifically, the POD for the RII ranged from 15% to 59% (53% to 73%) while the FAR ranged from 71% to 85% (53% to 79%) in the Atlantic (eastern North Pacific) basins, respectively, for the three RI thresholds studied. Nevertheless, the modest POD and relatively high FAR of the RII and other intensity guidance demonstrate the difficulty of predicting RI, particularly in the Atlantic basin.

1. Introduction

While some improvements have been made in operational tropical cyclone intensity forecasting in recent years (DeMaria et al. 2007), predicting changes in tropical cyclone intensity (as defined by the 1-min maximum sustained wind) remains problematic. Moreover, the operational prediction of rapid intensification (RI) has proven to be especially difficult (Elsberry et al. 2007) and, given the significant impacts of such episodes, has prompted the Tropical Prediction Center/National Hurricane Center (TPC/NHC) (NHC 2008) to declare it as its top forecast priority. The difficulty of forecasting RI stems from a general lack of understanding of the physical mechanisms that are responsible for these rare events. Generally speaking, researchers have attributed RI to inner-core, oceanic, and large-scale processes. While many of these processes are described in Kaplan and DeMaria (2003, hereafter KD03), a few of the more notable ones, as well as some that were described in the more recent literature, are summarized below.

The potential impacts of inner-core processes on RI have been examined by a number of researchers. The organization of the eyewall convection and the establishment of a region of high inertial stability near the storm center are fundamentally important to the intensification process (e.g., Schubert and Hack 1982). To illustrate,

Corresponding author address: John Kaplan, NOAA/AOML/Hurricane Research Division, 4301 Rickenbacker Cswy., Miami, FL 33149.
E-mail: john.kaplan@noaa.gov

DOI: 10.1175/2009WAF2222280.1

Willoughby et al. (1982) showed that large increases in tropical cyclone intensity sometimes occur as an outer eyewall contracts during a concentric eyewall cycle. More recently, Kossin and Schubert (2001) conducted simple barotropic numerical modeling simulations that showed the presence of mesovortices within the hurricane inner-core region can lead to large pressure falls provided that the magnitude and arrangement of the eyewall vorticity is favorable. Eastin et al. (2005a,b) suggest that the degree to which the eyewall mesovortices are able to mix high equivalent potential temperature air from the eye into the eyewall may play a key role in determining whether RI actually occurs. Most recently, Sitkowski and Barnes (2009) found a ''spiraling in'' of the eyewall during Hurricane Guillermo (1997) that yielded a smaller diameter and more complete eye that they speculated might have initiated the RI observed for that storm.

The potential role of the ocean in the RI process has also been investigated. One such observational study conducted by Shay et al. (2000) showed that Hurricane Opal (1995) intensified rapidly as it passed over a warm core eddy in the Gulf of Mexico. Although the coupled modeling results of Hong et al. (2000) confirmed that most of the intensification that occurred during that time period could be attributed to the presence of the eddy, their study showed that Opal still intensified rapidly in simulations conducted without the eddy. Thus, other physical mechanisms such as low vertical wind shear and enhanced divergence generated by an upper-level trough likely also played important roles in Opal's RI, as was hypothesized by Bosart et al. (2000).

The modeling simulations performed by Hong et al. (2000) showed that the net effect of the eddy that Opal encountered was to lessen the magnitude of the cooling of the sea surface temperature (SST) below the storm by about 0.5°C. This finding is consistent with the results of Cione and Uhlhorn (2003), who showed that systems intensified at greater rates when the underlying ocean cooled less. Thus, the primary impact of ocean eddies and other regions of high ocean heat content may be the reduction of storm-induced SST cooling in the storm's inner-core region, as noted by Mainelli et al. (2008).

The importance of large-scale environmental forcing on RI has been investigated by a number of researchers. One such study performed by Molinari and Vollaro (1990) showed that the rapid deepening in Hurricane Elena (1985) was proceeded by forcing from an upper-level trough. Their study showed that this interaction resulted in enhanced middle-level inflow, upper-level outflow, and stronger vertical motion near the storm's inner core. However, a later study performed by Hanley et al. (2001) found that RI is more likely to occur when there is no interaction between a tropical cyclone and an upper-level trough or cold low, suggesting that external forcing from troughs is likely a factor in the minority of RI cases. The importance of the vertical shear of the horizontal wind on RI has been illustrated by the modeling simulations of Frank and Ritchie (2001) and the observational results of KD03, both of which show that systems are more likely to undergo RI when embedded in regions of low vertical wind shear.

To better understand and ultimately predict RI, KD03 examined the large-scale environmental conditions that were conducive for Atlantic basin systems to undergo RI that they defined as a 24-h intensity increase of 15.4 m s^{-1} (30 kt). Their study showed that RI cases were typically embedded in an environment with lower vertical shear of the horizontal wind and higher lower-tropospheric relative humidity. KD03 also showed that systems that underwent RI were typically further from their maximum potential intensity, over warmer SSTs, and had been intensifying more in the previous 12 h than systems that did not undergo RI. These findings were subsequently used to develop a simple five-predictor RI index (RII) for estimating the probability of RI over the next 24 h for Atlantic basin systems. This early version of the RII was adopted for operational use in the Atlantic basin by the TPC/NHC prior to the 2003 hurricane season.

This paper describes the development of a revised version of the RII that employs more sophisticated statistical methods than were used in KD03, as well as some additional predictors. Since the original RII was developed exclusively for the Atlantic, a version is also developed for the eastern North Pacific basin. In addition, versions of the RII are developed for two other RI thresholds (25 and 35 kt) in addition to the 30-kt threshold that was employed in KD03. The revised versions of the RII are then verified on independent Atlantic and eastern North Pacific basin samples for all three RI thresholds.

2. Rapid intensification climatology

a. Atlantic basin RI distribution

The TPC/NHC Hurricane Database (HURDAT; Jarvinen et al. 1984) for the period 1989–2006 is used to obtain an updated RI climatology for the Atlantic basin. In the KD03 study, RI was defined as the 95th percentile of all 24-h overwater intensity changes of tropical cyclones of tropical depression intensity or greater. This corresponded to a 24-h increase in the maximum sustained wind of 30 kt (15.4 m s^{-1}) for the 1989–2000 KD03 sample. Although subtropical cases were excluded from KD03, they are employed in the present study since one of the requirements of TPC/NHC is to issue forecasts for these types of systems.

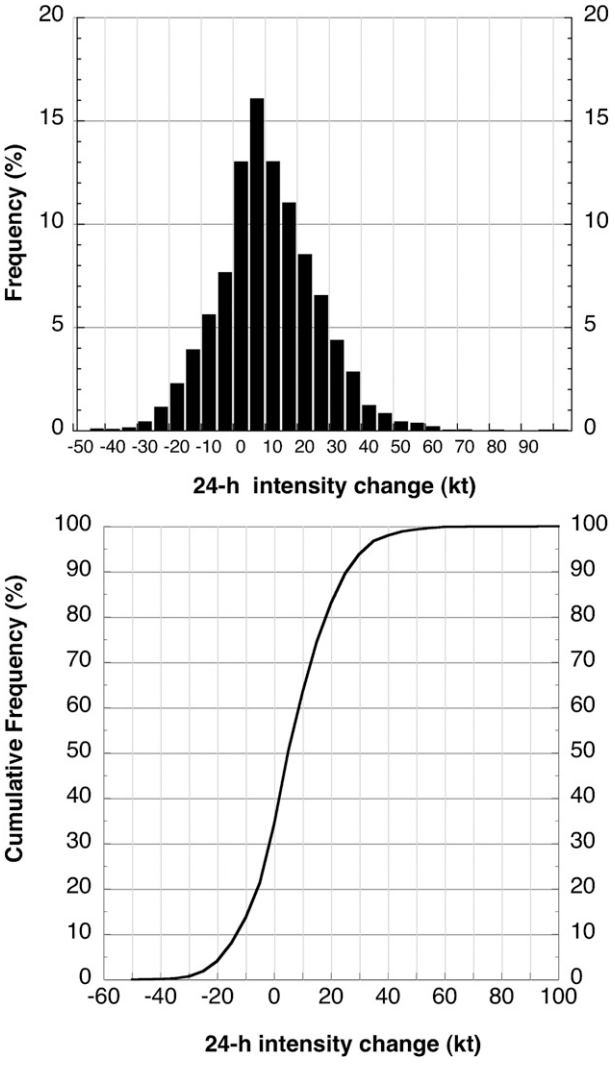

FIG. 1. (top) Frequency distribution and (bottom) cumulative frequency distribution of the overwater 24-h intensity changes of the 1989–2006 Atlantic basin sample.

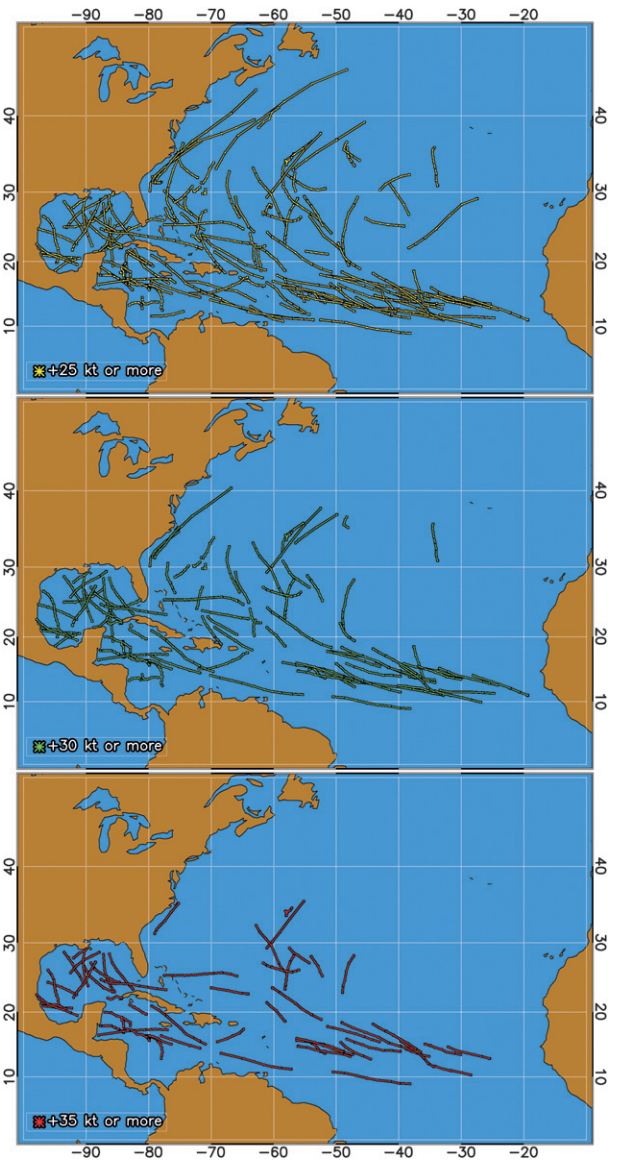

FIG. 2. The 24-h observed tracks of the Atlantic basin RI cases for the (top) 25- (yellow), (middle) 30- (green), and (bottom) 35-kt (red) RI thresholds.

Figure 1 indicates that the 30-kt RI threshold employed in KD03 represents about the 94th percentile of all Atlantic basin tropical and subtropical overwater 24-h intensity changes for the period 1989–2006. In the present study, RI indices are also derived for the 25- and 35-kt RI thresholds. These thresholds correspond to approximately the 90th and 97th percentiles of the Atlantic basin overwater intensity changes in Fig. 1, respectively. It should be noted that the 24-h Atlantic basin intensity distribution is skewed toward positive intensity changes. This may be due, in part, to an increased likelihood for Atlantic basin systems to make landfall and dissipate or to become extratropical since both outcomes would likely lessen the likelihood of capturing the entire life cycle of those systems.

Figure 2 shows the observed 24-h tracks of the Atlantic RI cases commencing at the start of each period of RI for all three RI thresholds. While the tracks of the RI cases for the 25- and 30-kt RI thresholds occur over a large portion of the Atlantic basin, the tracks of the RI cases that satisfy the 35-kt threshold tend to be more restricted in areal coverage, with very few cases occurring north of 30°N. The RI cases for the 35-kt RI threshold also tend to be somewhat more concentrated in the central Atlantic between 10° and 20°N and 20° and 60°W, as well as in the central and western portions of the Caribbean and the central Gulf of Mexico. Figure 3 indicates that the vast

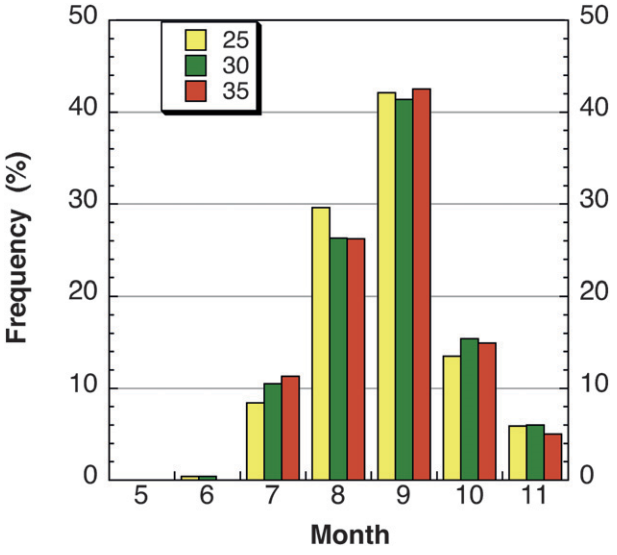

FIG. 3. Frequency distribution of the initial month of development of Atlantic RI cases for the 25- (yellow), 30- (green), and 35- (red) RI thresholds.

majority of RI cases occur in August and September with 71.7%, 67.7%, and 68.7% of the RI cases that satisfy the 25-, 30-, and 35-kt RI thresholds occurring during those months, respectively. Interestingly about 20% of all of the RI cases occur during the latter part (October and November) of the Atlantic hurricane season while only about 10% occur early in the hurricane season (June and July).

Table 1 shows the 24-h intensity changes of all of the Atlantic basin RI cases for systems that are initially of tropical depression, tropical storm, and hurricane intensity and for all tropical cyclones for each RI threshold. It can be seen that tropical depressions compose the smallest percentage of the RI cases (10.5%, 9.4%, and 7.1%, for the 25-, 30-, and 35-kt RI thresholds, respectively) while tropical storms compose the highest percentage (51.7%, 50.4%, and 47.5%) for those same three RI thresholds. This finding is partly due to the sample sizes of the three different intensity stratifications since there were 1952 tropical storm cases but only 1704 hurricane cases and 731 tropical depressions cases in the entire sample. However, the probability that a system will undergo RI (i.e., the total number of RI cases divided by the total number of cases for each stratification) (not shown) is still generally larger for tropical storms than hurricanes or tropical depressions for each of the thresholds. The exception is for the 35-kt RI threshold where the 3.8% probability of RI of the hurricane sample is slightly higher than the 3.4% probability of RI of the tropical storm sample.

Figure 4 shows the frequency distribution of all RI cases as a function of initial intensity. It can be seen that the distribution of RI cases for the 25- and 30-kt RI thresholds is skewed to the left, with cases with 35–40-kt initial intensities composing the largest fraction of RI cases. This result may be a reflection of the tendency for systems that are far away from their maximum potential intensity to exhibit fairly large rates of intensification. Interestingly, systems with initial intensities of 65–70 kt are the most likely to satisfy the 35-kt RI threshold. Perhaps, systems of this intensity are both sufficiently well organized and relatively far from their maximum

TABLE 1. The distribution of 24-h intensity changes (ΔV_{24}) of the Atlantic basin RI cases for the period 1989–2006. Distributions are shown for systems that are initially of tropical depression, tropical storm, and hurricane intensity and for the entire tropical cyclone sample. The total number of RI cases and percentage of the sample total (parentheses) contributed by each of the four intensity stratifications are provided at the bottom of the table for the 25- (RI_{25}), 30- (RI_{30}), and 35-kt (RI_{35}) RI thresholds.

ΔV_{24} (kt)	Tropical depression	Tropical storm	Hurricane	All tropical cyclones
25–30	23	103	66	192
30–35	15	67	43	125
35–40	9	27	18	54
40–45	0	18	19	37
45–50	1	9	9	19
50–55	0	4	12	16
55–60	0	6	3	9
60–65	0	0	1	1
65–70	0	1	1	2
70–75	0	0	0	0
75–80	0	1	0	1
80–85	0	0	0	0
85–90	0	0	0	0
90–95	0	1	0	1
95–100	0	0	1	1
Total cases RI_{25} (%)	48 (10.5)	237 (51.7)	173 (37.8)	458 (100.0)
Total cases RI_{30} (%)	25 (9.4)	134 (50.4)	107 (40.2)	266 (100.0)
Total cases RI_{35} (%)	10 (7.1)	67 (47.5)	64 (45.4)	141 (100.0)

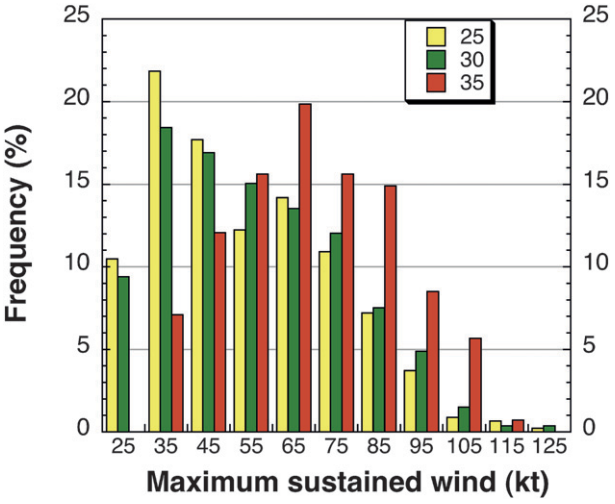

FIG. 4. Frequency distribution of the maximum wind at the start of each period of RI for the Atlantic basin for the 25- (yellow), 30- (green), and 35-kt (red) RI thresholds.

potential intensity, making it a relatively favorable intensity from which to undergo RI. It is worth noting that it is rather uncommon for category 3 or greater intensity hurricanes to undergo RI.

b. Eastern North Pacific basin RI distribution

For the period from 1989 to 2006, the 25-, 30-, and 35-kt RI thresholds correspond to about the 88th, 92nd, and 94th percentiles of the eastern North Pacific basin overwater intensity changes shown in Fig. 5, respectively, as determined from the HURDAT database. These values are about 2%–3% lower than the corresponding Atlantic basin RI percentiles indicating that higher overall intensification rates are found in the eastern North Pacific compared to the Atlantic basin. It should be noted that the eastern North Pacific basin intensity changes are more normally distributed than are the Atlantic basin changes shown in Fig. 1. This is likely due to a higher probability of capturing the entire life cycle of eastern North Pacific systems due to the lower likelihood of systems making landfall or become extratropical in that basin. Thus, the finding that the three RI thresholds are lower in the eastern North Pacific basin than the Atlantic is even stronger since had the Atlantic intensity distribution been more normally distributed, like that of the eastern North Pacific, the corresponding percentiles of the Atlantic basin RI thresholds would have been even higher. This is true since making the Atlantic distribution more normal would require the inclusion of more negative intensity changes and this would result in the RI cases representing a smaller fraction of the cases and hence a higher percentile of the total Atlantic sample.

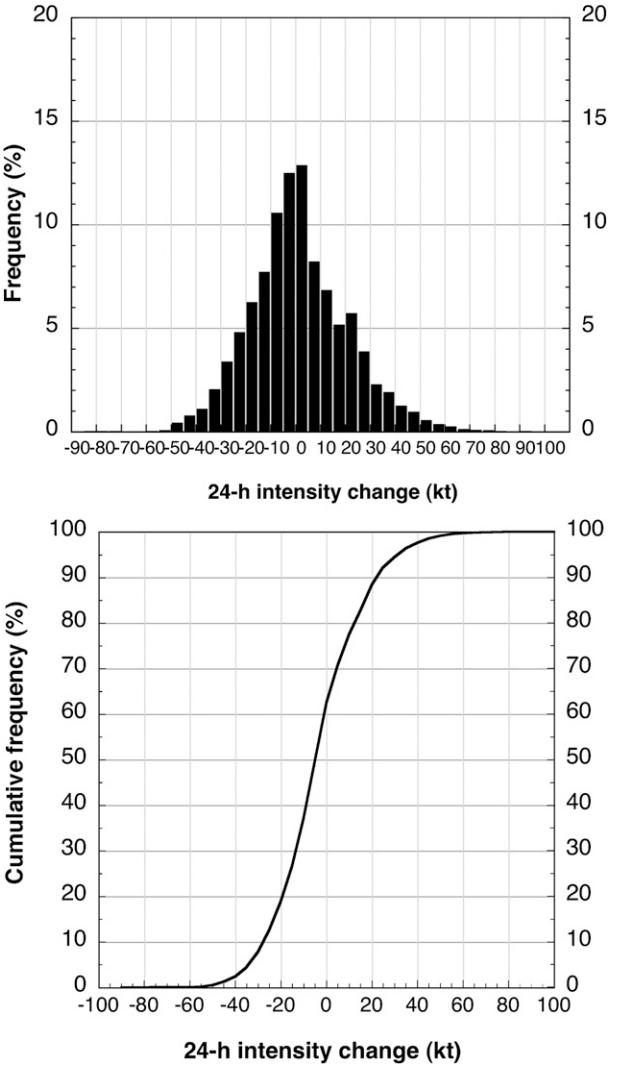

FIG. 5. As in Fig. 1, but for the eastern North Pacific basin.

It should be noted that the eastern North Pacific basin, as defined in this study, also includes the region between 140° and 160°W. Although operationally this area is typically considered part of the central Pacific basin, it is assumed to be part of the eastern North Pacific basin in our study since the Hawaiian Islands are located there. However, since the cases from that region only represent about 1% of the total sample for that region, the inclusion of this area should have little impact on the overall eastern North Pacific basin statistics.

Figure 6 shows the tracks of the eastern North Pacific RI cases for each RI threshold. It can be seen that RI cases are clustered in the region between approximately 10°–20°N and 95°–140°W with about 94% of all of the RI cases occurring in this region. The concentration of the eastern North Pacific RI cases is in strong contrast to the more widespread regions of RI development found for

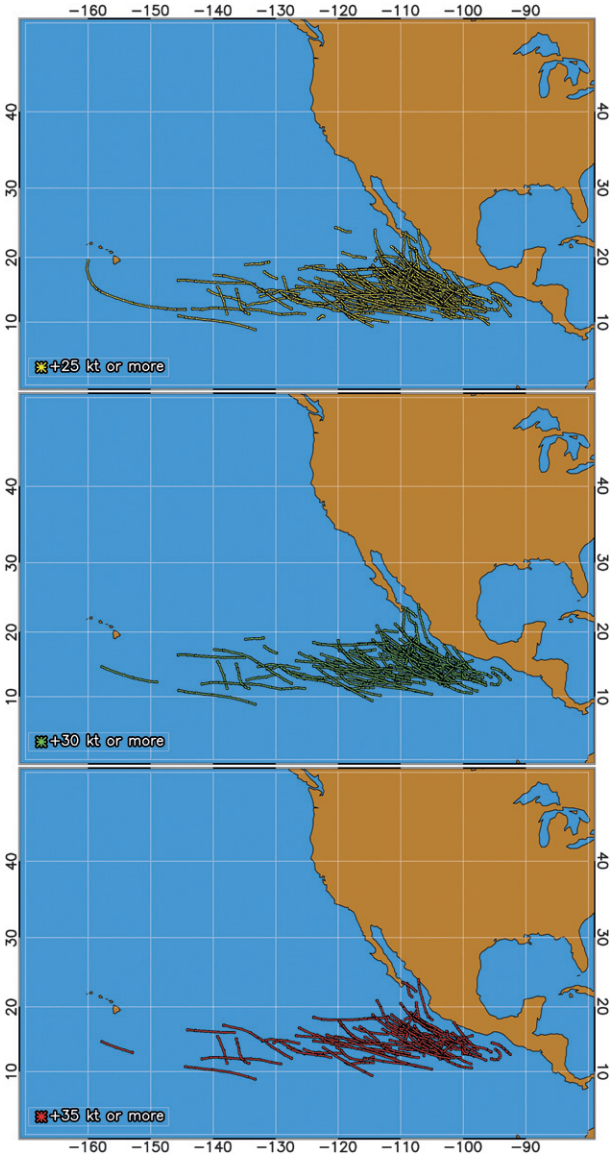

FIG. 6. As in Fig. 2, but for the eastern North Pacific basin.

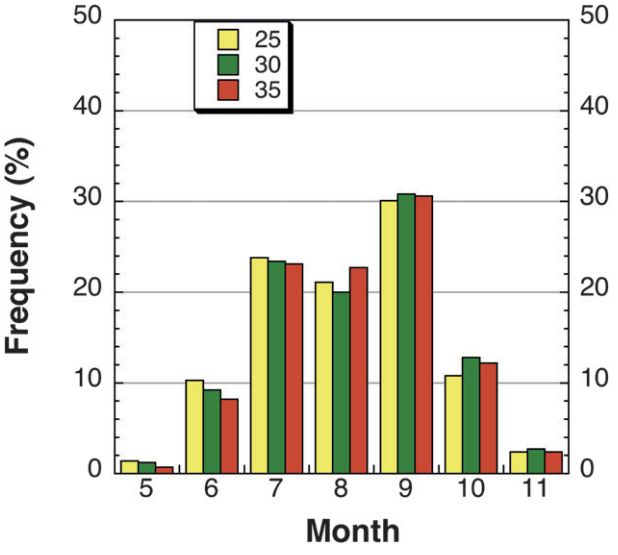

FIG. 7. As in Fig. 3, but for the eastern North Pacific basin.

the Atlantic basin (Fig. 2) and is consistent with the results of Gray (1968) that showed a similarly large concentration of tropical cyclone genesis occurrences in that same region. The high concentration of eastern North Pacific RI cases is likely due, in part, to the existence of much more favorable thermodynamics in that area, since Levitus (1982) has shown that SSTs typically decrease rapidly outside this region and these lower SSTs would presumably be associated with drier, more stable conditions that are less conducive for a system to intensify. In addition, the absence of the Saharan air layer (SAL) may also be responsible for the high concentration of RI cases in that region. The SAL is characterized by dry stable air that is generally considered to be less conducive for tropical cyclone intensification and Dunion and Velden (2004) found that the SAL usually does not extend into the east Pacific basin. Thus, westward-moving tropical waves might experience an increased likelihood of undergoing RI after exiting the Atlantic and entering the eastern North Pacific basin.

Figure 7 indicates that the month with the highest percentage of RI cases in the eastern North Pacific is September, which is in agreement with the Atlantic basin results discussed previously (Fig. 3). However, about twice as many RI cases occur during the months of June and July compared to the months of October and November in the eastern North Pacific, whereas in the Atlantic the activity during these earlier months is only half of what it is for the latter ones. Perhaps the lack of early RI activity in the Atlantic basin is due to a higher likelihood for systems to be embedded in the SAL during that time period, since Dunion and Marron (2008) recently found that the SAL is much more prevalent in the early months of the Atlantic hurricane season. The lack of early RI activity in the Atlantic is also consistent with the results of DeMaria et al. (2001) that indicate that midlevel moisture reaches a minimum in July in the Atlantic basin.

Table 2 shows the distribution of the 24-h intensity changes of the eastern North Pacific basin cases for the intensity stratifications that were examined previously for the Atlantic basin. It can be seen that systems that are initially of tropical storm intensity accounted for approximately 60% of the RI cases for each of the RI thresholds. As was noted previously, the higher number of RI cases that are initially of tropical storm intensity is partly due to differences in the sample size since there

TABLE 2. As in Table 1, but for the 1989–2006 eastern North Pacific sample.

ΔV_{24} (kt)	Tropical depression	Tropical storm	Hurricane	All tropical cyclones
25–30	35	115	56	206
30–35	12	75	34	121
35–40	16	52	33	101
40–45	2	42	22	66
45–50	1	32	18	51
50–55	0	19	10	29
55–60	0	11	8	19
60–65	0	10	3	13
65–70	0	3	3	6
70–75	0	2	2	4
75–80	0	3	0	3
80–85	0	0	1	1
85–90	0	0	0	0
90–95	0	0	1	1
95–100	0	0	0	0
Total cases RI_{25} (%)	66 (10.6)	364 (58.6)	191 (30.8)	621 (100.0)
Total cases RI_{30} (%)	31 (7.5)	249 (60.0)	135 (32.5)	415 (100.0)
Total cases RI_{35} (%)	19 (6.4)	174 (59.2)	101 (34.4)	294 (100.0)

were 2439 tropical storm cases and only 1894 hurricane and 1002 tropical depression cases. Nevertheless, the probability of RI, which accounts for variations in sample size, is still larger for tropical storms than it is for either tropical depressions or hurricanes for each of the three RI thresholds.

Figure 8 shows the distribution of RI cases as a function of initial intensity for the three RI thresholds. Figure 8 shows that systems that are initially of weak tropical storm intensity (35–40 kt) are more likely to undergo RI at the 25- and 30-kt RI thresholds, while strong tropical storms (55–60 kt) are more likely to undergo RI at the 35-kt RI threshold. Perhaps, strong tropical storms are more likely to undergo RI at the highest RI threshold since they are likely to be both fairly well organized and relatively far from their maximum potential intensity.

3. Derivation of the RII for the Atlantic and eastern North Pacific basins

A revised RII for the Atlantic and a new RII for the eastern North Pacific basin are developed using atmospheric and oceanic predictors from the Statistical Hurricane Intensity Prediction Scheme (SHIPS) (DeMaria et al. 2005). The SHIPS atmospheric predictors are determined from gridded 2° × 2° latitude–longitude (2.5° × 2.5° prior to 1996) fields from the operational global analysis produced at the National Centers for Environmental Prediction (NCEP). These fields are available four times a day (0000, 0600, 1200, and 1800 UTC) from 2000 to the present, and twice a day (0000 and 1200 UTC) prior to then. The SST is determined from a weekly gridded 1° × 1° analysis (Reynolds and Smith 1993). Additional predictors are determined from satellite data archived at the Cooperative Institute for Research in the Atmosphere (CIRA). These predictors are computed from channel-4 (10.7 μm) infrared (IR) imagery from Geostationary Operational Environmental Satellites (*GOES-East* and *-West*) for systems that developed in the Atlantic and eastern North Pacific basins since 1995, as described in Mueller et al. (2006). An additional predictor is the oceanic heat content (OHC) derived from surface height altimetry data, weekly SST analyses, and a seasonal mean ocean climatology using the methodology of Mainelli et al. (2008).

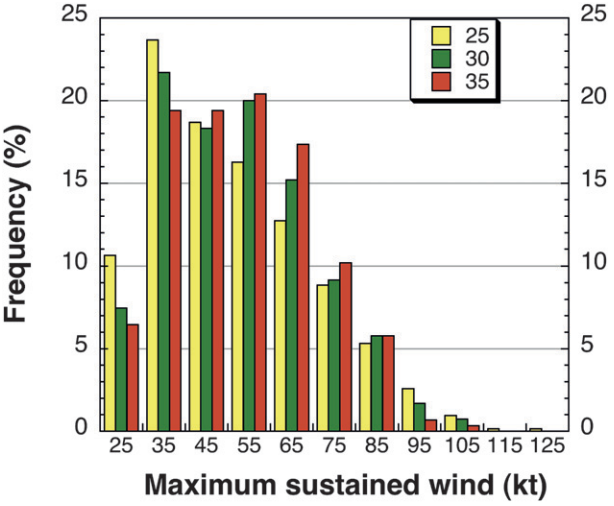

FIG. 8. As in Fig. 4, but for the eastern North Pacific basin.

TABLE 3. The predictors used in the revised Atlantic RII index.

Predictor	Definition
PER	Previous 12-h intensity change
SHRD	850–200-hPa vertical shear of the horizontal wind from the 0–500-km radius
D200	200-hPa divergence from the 0–1000-km radius
RHLO	850–700-hPa relative humidity from 200–800-km radius
PX30	Percent area from 50 to 200 km covered by ≤ -30°C IR cloud-top brightness temperatures
SDBT	Std dev of 50–200-km IR cloud-top brightness temperatures
POT	Potential intensity (current intensity − maximum potential intensity)
OHC	Ocean heat content

a. Atlantic basin RII

1) SELECTION OF ATLANTIC RI PREDICTORS

The predictors selected for use in the Atlantic basin RII are similar to those that were employed in the original version described in KD03. The predictors in the original version of the RII were the vertical shear of the horizontal wind between 850 and 200 hPa (SHRD), relative humidity between 850 and 700 hPa (RHLO), potential intensity (POT), SST, and previous 12-h change in intensity (PER). The values of SHRD, RHLO, SST, and POT were all evaluated at $t = 0$ h, while PER was evaluated for the 12-h period prior to time $t = 0$ h. These predictors were originally chosen from a group of predictors for which it had been shown that statistically significant differences existed at the 99.9% level between the mean values of the RI and non-RI samples based upon a two-sided Behrens–Fisher t test, which assumes unequal sample variances (Dowdy and Wearden 1991).

The predictors employed in the revised RII include four predictors (SHRD, RHLO, POT, and PER) that were utilized in the KD03 version as well as four new predictors (one large-scale predictor and three satellite-derived predictors). Specifically, the 200-hPa divergence (D200) averaged from 0- to 1000-km radius from the storm center, the percentage area from 50- to 200-km radius covered by IR cloud-top brightness temperatures of −30°C or colder (PX30), the standard deviation of IR cloud-top brightness temperature (SDBT) over that same region, and the OHC are all utilized. Similar to the variables used in the original RII, statistically significant differences at the 99.9% level were found between the RI and non-RI samples for each of these variables for all three RI thresholds. Other statistically significant predictors were also tested for use in the RII; however, the aforementioned variables were chosen since they yielded the most skillful RII by measures discussed later in this section. Table 3 shows a list of the predictors used in the revised Atlantic RII.

Although as noted above, four of the predictors in the revised RII are the same as those in the KD03 version, some of these were evaluated in a slightly different manner than was employed previously. In the current version of the RII, SHRD is evaluated from 0- to 500-km radius from the storm center after first removing the storm vortex from the NCEP analysis, as described in Knaff et al. (2009), while previously it was computed from 200- to 800-km radius from the storm center without first removing the storm vortex. The POT was also evaluated in a slightly different manner than was used in KD03. Previously, POT was determined by subtracting the current storm intensity from the empirically derived maximum potential intensity (DeMaria and Kaplan 1994) using SSTs determined from the weekly Reynolds and Smith (1993) analysis. However, in the revised RII the maximum potential intensity is determined using an adjusted (i.e., cooled) inner-core SST computed using an algorithm derived exclusively for the Atlantic basin by Cione et al. (2009). The Cione et al. inner-core cooling algorithm is a function of storm speed, latitude, and initial SST with fast-moving low-latitude storms exhibiting the least amount of cooling and slow-moving high-latitude storms the most. This algorithm has been used in the operational Atlantic basin version of SHIPS since the 2006 hurricane season.

Another difference between the current and original versions of the RII is that the large-scale predictors utilized in the original version were evaluated at time $t = 0$ while those in the revised RII (SHRD, RHLO, POT, D200, and OHC) are averaged along the storm track from $t = 0$ to $t = 24$ h. When run operationally, the 24-h average values of SHRD, RHLO, and D200 are computed from the NCEP forecast fields while the OHC evaluated at the storm center is averaged along the storm track using the $t = 0$ h analysis of this predictor. However, both of the GOES predictors (PX30 and SDBT) are only evaluated at $t = 0$ h since model forecasts of these quantities are not available. Finally, POT is evaluated along the storm track using the $t = 0$ h SST analysis while PER is evaluated for the 12-h period prior to $t = 0$ h.

The revised Atlantic RII is derived using data from 1995 to 2006 (1995 was the first year that *GOES-8*

TABLE 4. Mean magnitudes of the Atlantic basin RI predictors for the RI and non-RI samples for the (a) 25-, (b) 30-, and (c) 35-kt RI thresholds. The differences between the means of the RI and non-RI samples and the statistical significance of these differences are also noted at the 99.9th (bold), 95th (*), and 90th (+) percent level, respectively. The sample sizes for the RI (non-RI samples) for the 25-, 30-, and 35-kt RI thresholds are $N = 255$ (1500), $N = 155$ (1506), and $N = 91$ (1451), respectively.

(a)

Predictor	Units	RI (mean)	RI (std dev)	Non-RI (mean)	Non-RI (std dev)	RI–non-RI (mean)
PER	m s^{-1}	4.0	4.4	1.3	4.3	**2.7**
D200	10^{-7} s^{-1}	46.9	28.8	24.7	31.3	**22.2**
SHRD	m s^{-1}	5.4	2.4	8.2	4.2	**−2.8**
RHLO	%	73.1	6.2	68.7	6.9	**4.4**
POT	m s^{-1}	40.6	12.5	35.5	13.9	**5.1**
OHC	KJ cm^{-2}	55.4	31.7	36.9	28.3	**18.5**
SDBT	°C	13.7	6.0	16.9	6.7	**−3.2**
PX30	%	76.6	20.9	57.8	27.4	**18.8**

(b)

Predictor	Units	RI (mean)	RI (std dev)	Non-RI (mean)	Non-RI (std dev)	RI–non-RI (mean)
PER	m s^{-1}	4.3	4.7	1.5	4.3	**2.8**
D200	10^{-7} s^{-1}	49.2	30.0	25.6	31.5	**23.6**
SHRD	m s^{-1}	5.1	2.0	8.0	4.2	**−2.9**
RHLO	%	73.5	6.2	69.1	6.9	**4.4**
POT	m s^{-1}	39.7	11.3	37.3	13.3	2.4*
OHC	KJ cm^{-2}	55.3	30.0	39.0	29.9	**16.3**
SDBT	°C	12.5	5.4	17.1	6.7	**−4.6**
PX30	%	79.5	20.2	57.6	27.2	**21.9**

(c)

Predictor	Units	RI (mean)	RI (std dev)	Non-RI (mean)	Non-RI (std dev)	RI–non-RI (mean)
PER	m s^{-1}	4.5	5.2	3.2	4.2	**1.3**
D200	10^{-7} s^{-1}	50.7	29.6	26.3	31.3	**24.4**
SHRD	m s^{-1}	4.7	1.7	7.9	4.1	**−3.2**
RHLO	%	73.9	5.8	69.4	7.0	**4.5**
POT	m s^{-1}	40.9	10.3	39.0	12.4	1.9+
OHC	KJ cm^{-2}	61.4	300.8	40.9	29.0	**20.5**
SDBT	°C	12.2	5.5	17.2	6.8	**−5.0**
PX30	%	82.5	17.0	57.3	27.1	**25.2**

satellite data were archived at CIRA). For this period, there are a total of 2140 overwater 24-h RI and non-RI forecast times for which all eight RI predictors are available. Prior to the selection of the final cases for deriving the RI indices, this sample was subjected to additional screening procedures. First, only cases for which POT is at least as large as the RI threshold are considered for use in the derivation of the RII. For example, when deriving the RI index for the 25-kt RI threshold, only cases with POT $\geq$ 25 kt are included in the final developmental sample.

In addition, cases where the values of any of the eight RI predictors were outside the range of RI predictor magnitudes of the RI cases in the developmental sample are not utilized when deriving the RII. For example, the SHRD of all RI cases for the 30-kt RI threshold are $\leq$12.3 m s^{-1}. Thus, any case in the developmental sample with SHRD $>$12.3 m s^{-1} is excluded from the dataset used to derive the RII. The same methodology was utilized to ensure that each of the other seven RI predictors of a given case were within the range of the observed RI predictor magnitudes of the RI cases in the developmental sample. The decision to exclude any case with RI predictor magnitudes that were outside the range of observed RI values was made since sensitivity tests showed that doing so yielded a more skillful RII when evaluated for the entire 2140-case developmental sample.

Table 4 shows the average magnitude of the RI and non-RI samples for each of the RI thresholds for the final screened sample that is used to derive the revised Atlantic RII. The differences between the means, as well as the statistical significance of these differences, are also provided. It can be seen that statistically significant differences at the 99.9% level are found for all three RI thresholds for nearly every predictor. The lone exception is for the POT predictor where the differences

are significant at the 95th and 90th percentiles for the 30- and 35-kt RI thresholds, respectively. The lower significance for the POT predictor is likely the result of the aforementioned screening technique that excluded cases with POT values below the RI threshold, since significance tests performed on the full (2140 case) developmental sample showed statistically significant differences at the 99.9% level between the RI and non-RI samples for all three RI thresholds for this predictor.

In general, the differences between the RI and non-RI samples are consistent with physical reasoning and previous research. The higher values of PER for RI cases seems reasonable since systems that are undergoing relatively large rates of intensification are likely to be fairly well organized, while the finding of larger values of POT is consistent with an enhanced potential for systems with intensities that are further from their maximum potential intensity to undergo RI. Furthermore, the higher values of OHC for RI systems appear to be consistent with the results of Mainelli et al. (2008), who showed that systems were more likely to become intense when located over regions of high OHC.

Table 4 also indicates that RI cases have larger values of D200 and RHLO, but lower values of SHRD. The finding of lower vertical shear and higher low-level humidity for RI cases is consistent with the observational results of KD03, while the larger values of upper-level divergence observed for RI cases is in agreement with the findings of Bosart et al. (2000), as noted previously. Finally, the RI cases are shown to have higher values of PX30 and lower values of SDBT. These results indicate that deep convective clouds in RI systems tend to be both more widespread and symmetric. The former finding is consistent with physical reasoning, while the latter agrees with the modeling results of Nolan and Grasso (2003) that showed that asymmetric convective heating had a negative impact on a storm's overall intensity. It is worth noting that the variations in predictor magnitude between RI thresholds also seem consistent with physical reasoning. Specifically, PER, D200, RHLO, POT, PX30, and OHC all become larger as the magnitude of the RI threshold increases while SHRD and SDBT decrease.

2) Derivation of the Atlantic RII

In the original RII developed in KD03, RI thresholds were employed to assess the likelihood of RI. These thresholds were equal to the average magnitude of each of the five RI predictors for all cases that underwent RI. The RI threshold for each predictor was said to have been satisfied if the observed predictor magnitude for a given case was either greater than or equal to or less than or equal to the RI threshold, whichever statistical analysis performed on the developmental sample had shown to be more favorable. The probability of RI was then determined by computing the percentage of all cases that satisfied one, two, three, four, and five thresholds that underwent RI for that 24-h forecast period. Further details about the methodology used to derive the original RII are provided in KD03.

A weakness of the original KD03 ''threshold'' version of the RII was that it was not possible to account for the degree to which conditions were either favorable or unfavorable since an RI threshold was either satisfied or not satisfied. To correct this problem, a new version of the RII is developed. This version uses the scaled magnitudes of the eight RI predictors to determine the likelihood of RI where each of the predictors is assigned a scaled value between 0 (least conducive) and 1 (most conducive) for RI. The scaled predictor values (S_p) are determined using the observed range of predictor values over which RI is observed to occur for each predictor.

To illustrate, the SHRD values for all of the 30-kt RI cases ranges from 1.5 to 12.3 m s^{-1}. Since both KD03 and the results in Table 4 indicate that low values of SHRD are most conducive to RI, a scaled value of 0.0 is assigned to a case for shear values $\geq$12.3 m s^{-1} while a scaled value of 1.0 is assigned for SHRD values of $\leq$1.5 m s^{-1}. Linear interpolation is used for cases with SHRD values between 1.5 and 12.3 m s^{-1}, so $S_p = 0.5$ for SHRD of 6.9 m s^{-1}. The above scaling methodology is employed to obtain S_p values for all eight RI predictors and these are then summed to obtain a single scaled value for each of the RI and non-RI 24-h forecast cases using

$$R_S = \sum_{n=8}^{n=1} S_{p_n}, \tag{1}$$

where S_{p_n} is the scaled magnitude of each of the eight RI predictors and R_s is the total scaled value of each forecast case. For cases when $S_p = 0$ for any of the individual RI predictors, R_s is set to 0 since it is assumed that the likelihood for a system to undergo RI is remote if any individual value of S_p is 0. It should be noted that, to combine the data using (1), the statistics of the S_p should be fairly similar. As a test of this assumption, an analysis of the distributions of the S_p values of the eight RI predictors is performed for the 30-kt RI threshold. This analysis indicates that the sample mean magnitude and standard deviation of each of the individual predictors are within about 10%–15% of the average magnitude (0.5) and average standard deviation (0.24) that is computed from all eight of the RI predictors. Furthermore, the distributions of the S_p value of the individual predictors are fairly normal although a few were somewhat skewed. A similar

analysis performed for the eastern North Pacific basin yielded similar results. Thus, the use of (1) to combine the S_p values seems like a fairly reasonable approach.

The R_S values of each of the 24-h forecast cases in the developmental sample are placed into quartiles with the lowest R_S values placed in the first quartile. The minimum and maximum R_S values of each quartile are chosen such that an equal number of RI cases rather than an equal number of total (RI + non-RI) cases are placed in each quartile. This technique was employed since it produced smoother variations in RI probabilities between quartiles and a more skillful RII. The probability of RI is then computed for each quartile by dividing the number of RI cases by the total number (RI + non-RI) of cases in each of the four quartiles. The above methodology is used to compute RI probabilities for all three RI thresholds for the ''scaled'' version of the RII.

While the aforementioned scaling technique accounts for how conducive for RI the conditions are for a given RI predictor, it does not account for the relative importance of each predictor to RI. Thus, a linear discriminant analysis (Wilks 1995) is performed to obtain weights for each of the RI predictors. Although the discriminant analysis could have been performed directly on each of the RI predictors without first scaling the data, the decision was made to conduct the discriminant analysis on the S_p values of the individual predictors to enable a more direct comparison of the skill of both techniques. Prior to performing the discriminant analysis, the cases for which $R_s = 0$ are excluded from the developmental sample since it was found that this yielded a more skillful RII. The weights (W_n) of each of the RI predictors, which are actually just the values of the linear discriminant vector ($\mathbf{d}_1$) as described in Wilks (1995), are then multiplied by the S_p values in (1) using

$$R_d = \sum_{n=1}^{n=8} W_n S_{p_n}, \qquad (2)$$

where R_d are the discriminant values of each case. It is important to note that an underlying assumption that is made when employing linear discriminant analysis is that the covariance matrices of the two groups (RI and non-RI in our study) are equal (Wilks 1995). An analysis of the covariance matrices of the Atlantic RI and non-RI samples for the 30-kt threshold indicates that their structures are indeed similar, with most of the elements of the two matrices being of comparable magnitude and sign. A similar analysis conducted on the eastern North Pacific basin RI and non-RI samples yielded similar results. Thus, although the matrices of the RI and non-RI groups are not an exact match, as is typically the case with real data, they appear to be similar enough to make this a reasonable assumption.

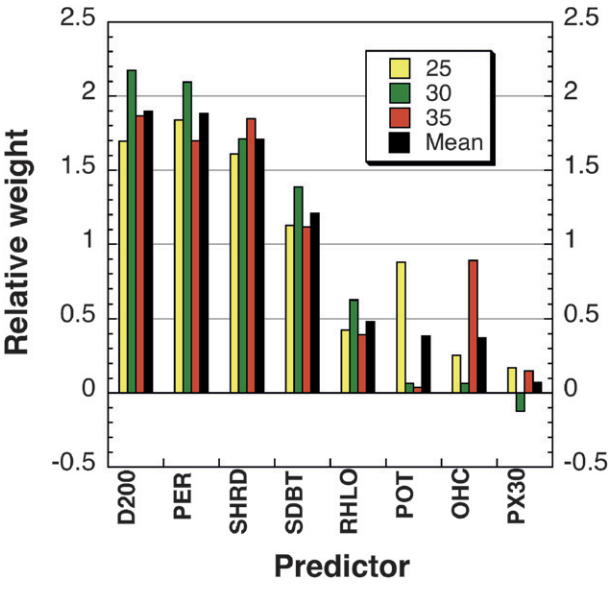

FIG. 9. The relative weights of the Atlantic basin RI predictors for the 25- (yellow), 30 - (green), and 35-kt (red) RI thresholds. The mean weights (black) of the three RI thresholds are also shown for each of the RI predictors.

Figure 9 shows the W_n of the RI predictors for each RI threshold. The mean W_n obtained by averaging the W_n for all three RI thresholds is also shown for each predictor. It can be seen that the W_n of the individual RI predictors can be quite different since the W_n of each predictor would be 1 if they were of equal importance. It can also be seen that the kinematic predictors (D200 and SHRD) as well as PER have at least twice the weight of the thermodynamic predictors (POT, RHLO, and OHC) for all three RI thresholds. It is also worth noting that the relative importance of each predictor can vary between RI thresholds. Interestingly, SDBT has a significantly greater weight than PX30, suggesting that the symmetry of the deep convection is much more important than the quantity, which is consistent with the aforementioned results of Nolan and Grasso (2003). It is important to note that an analysis of the correlation matrix for the S_p values for the 30-kt RI threshold indicates that nearly all of the predictors are only weakly correlated with the variance explained (r^2) between predictors being <0.2, although moderate correlations ($0.2 < r^2 < 0.6$) are observed between PX30 and SDBT and RHLO and D200. An analysis performed on the eastern North Pacific sample employed below yielded similar results. Thus, the W_n of most of the RI predictors should not be significantly impacted by the existence of the other predictors.

For operational forecasting purposes, it is desirable to estimate the probability of RI for a given case. One method for computing such probabilities would be to scale the discriminant function values obtained from (2) to a value between 0 and 1 and then to employ those values directly to compute the RI probabilities. However, this method introduces a high bias so an alternative procedure described below is used that ensures that the probabilities match those of the developmental sample.

The first step in computing the RI probabilities using this alternative method is to place the R_d values computed from (2) into quartiles following the same methodology that was used to derive the ''scaled'' version of the RII. The minimum and maximum R_d of each of the four quartiles are then determined such that an equal number of RI cases are placed in each quartile and the RI probabilities are computed by dividing the total number of RI cases in each quartile by the total number of cases (RI + non-RI) in that same quartile. Since an equal number of RI cases are placed in each quartile, the probabilities computed reflect the probability of RI for 25% of the RI cases. Although other binning techniques were used to compute RI probabilities, this methodology was employed since sensitivity tests showed that it produced a more skillful RII and smoother probability variations between quartiles. Also, the probability is assumed to be 0% when $R_d = 0$. The above technique is used to obtain RI probabilities for the ''discriminant'' version of the RII for the 25-, 30-, and 35-kt RI thresholds.

Figure 10 shows the variation in the probability of RI for each of the three RI thresholds for the ''discriminant'' version of the RII. The probabilities obtained for the scaled version of the RII discussed previously (not shown) are generally lower than those in Fig. 10. It can be seen that the RI probabilities are generally lowest (highest) for the first (fourth) quartile with the lowest (highest) R_d values. On average, the probabilities are highest for the 25-kt threshold and lowest for the 35-kt threshold, although the highest quartile four probabilities are found for the 30-kt threshold. The latter result is due, in part, to the use of the screening technique that excludes cases with POT values below the RI threshold when deriving the RII, since this resulted in slightly different samples being used to derive the three versions of the RII.

The climatological probabilities of RI are also shown for each RI threshold to provide a measure of the likelihood that RI will occur for any given 24-h forecast period. These are computed by dividing the number of RI cases for each of the three thresholds by the total number of cases in the full (2140 case) 1995–2006 developmental samples. The climatological RI probabilities are 12.0%, 7.3%, and 4.3% for the 25-, 30-, and 35-kt RI thresholds, respectively, for this time period. It can be seen that the RI probabilities for the second quartile are a factor of 2 greater than climatology while the probabilities computed for the fourth quartile are between 4 and 10 times greater.

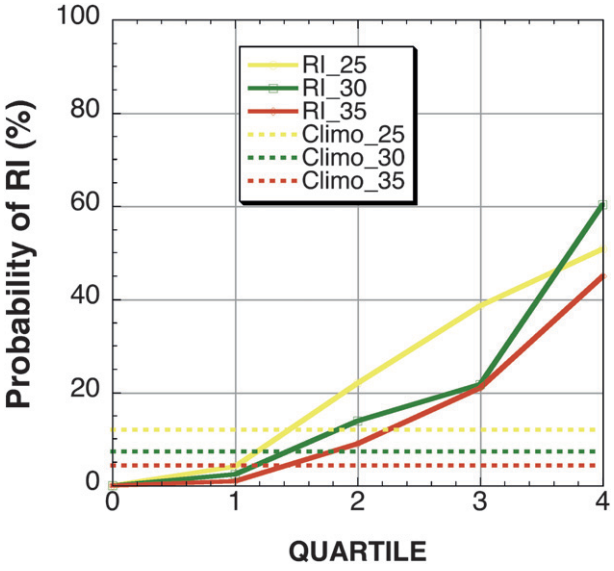

FIG. 10. The probability of RI for the Atlantic basin 25- (yellow), 30- (green), and 35-kt (red) RI thresholds for the discriminant RII. The climatological RI probabilities (dashed lines) are also shown for each RI threshold.

The skill of the RII forecasts made for the 1995–2006 developmental sample is assessed by computing the Brier score (BS) (Wilks 2006) of those forecasts and comparing it to the BS of forecasts computed based on the climatological probability of RI. To accomplish this, the probability of RI is first obtained by converting the R_s and R_d values of each developmental forecast case to RI probabilities (0 to 1) by linearly interpolating between the quartile average R_d, R_s, and RI probabilities of the scaled (not shown) and discriminant (Fig. 10) versions of the RII. The above procedure is employed to compute RI probabilities for all three RI thresholds. The probability values are then subtracted from 0 for cases when RI is not observed and 1 for cases when RI is observed for that forecast period and then squared. For example, for a 24-h time period when RI is observed, a forecast probability of 50% would yield a BS = 0.25 [i.e., $(0.50 - 1.0)^2$]. The aforementioned values are then summed to get the BS for both the scaled and discriminant versions of the RII. The same methodology is also used to obtain the BS for the climatological forecasts. When assessing those forecasts, the probability of RI is assumed to be a constant value equivalent to the climatological probability of RI (e.g., 12.0% for the 25-kt RI threshold).

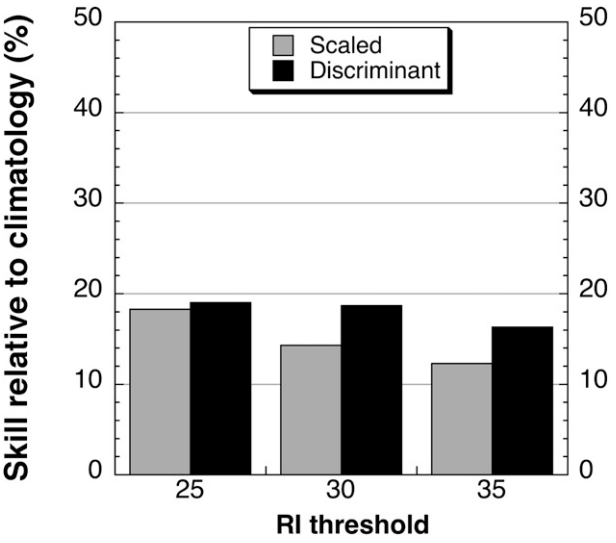

FIG. 11. The skill of the scaled and discriminant versions of the Atlantic basin RII relative to forecasts based upon climatology for the 1995–2006 developmental sample. The skill levels are shown for the 25-, 30-, and 35-kt RI thresholds. The sample size is 2140.

The skill of the scaled or discriminant RII is then evaluated using the Brier skill score (BSS) (Wilks 2006):

$$\mathrm{BSS} = \left[1 - \left(\frac{\mathrm{BSM}}{\mathrm{BSC}}\right)\right] \times 100, \qquad (3)$$

where BSM is the Brier score of the RII forecasts and BSC is the Brier score of the climatological forecasts. Thus, positive values of BSS indicate that the RII exhibited skill relative to climatology while negative values indicate that the RII was not skillful. Since (3) is expressed as a percentage, a BSS of 100% denotes perfect skill in this study. Figure 11 depicts the skill of the RII for both the discriminant and scaled versions of the RII for the 1995–2006 developmental data sample. It can be seen that both are skillful and that the discriminant version is more skillful than the scaled version for all three RI thresholds. Also, the skill of the RII decreases as the RI threshold increases.

b. Eastern North Pacific RI index

1) SELECTION OF EASTERN NORTH PACIFIC RI PREDICTORS

An eastern North Pacific version of the RII is also developed using the same methodology and nearly the same predictors as was employed in the Atlantic. However, since the OHC is not available for the eastern North Pacific basin, only the first seven RI predictors in Table 3 are used to derive the eastern North Pacific RII. Also, the POT variable is evaluated utilizing weekly SSTs (Reynolds and Smith 1993) rather than adjusted SSTs, since the Cione et al. (2009) algorithm that had been previously employed for use in the Atlantic RII was derived only for use in the Atlantic basin.

Table 5 shows the average magnitudes of the predictors of the RI and non-RI samples for the seven predictors that were used to derive the eastern North Pacific RII. The differences between the RI and non-RI cases are similar to those that were found in the Atlantic basin. Specifically, the RI cases are intensifying faster than the non-RI cases (larger values of PER) and have higher values of D200, RHLO, POT, and PX30, as well as lower values of SHRD and SDBT. The differences between the mean magnitudes of the RI and non-RI cases for each of these variables are significant at the 99.9% level for each RI threshold.

It is worth noting that, on average, systems that intensify by the largest RI threshold (35 kt) have the largest values of PER, D200, RHLO, and PX30 and lowest values of SHRD and SDBT. Although these differences are not that large, they are consistent with physical reasoning. A slightly lower POT was also found for cases that satisfy the highest RI threshold. Although this is somewhat counterintuitive, it likely results, in part, from the screening methodology, which excludes cases based upon their POT value, as was noted previously.

2) DERIVATION OF THE EASTERN NORTH PACIFIC RII

Figure 12 shows the weights of the seven eastern North Pacific RI predictors for each RI threshold determined based upon linear discriminant analysis (Wilks 2006). It can be seen that the PER, SDBT, and POT predictors have the largest weights of all of the predictors. These results contrast with those from the Atlantic basin where D200, PER, and SHRD were found to be the most important predictors. An analysis of the mean SHRD and D200 of all cases in the eastern North Pacific and Atlantic basins indicates that these variables are, on average, more favorable (lower SHRD and higher D200 values) and less variable (lower standard deviation) in the eastern North Pacific basin than the Atlantic basin. Thus, the lower relative weights of SHRD and D200 in the eastern North Pacific are likely due to a general increased likelihood of finding favorable values of those variables in that basin as opposed to a lower overall importance.

The probability of RI for the eastern North Pacific cases is computed using the same methodology that was employed for the Atlantic basin. Figure 13 shows the RI probabilities of the discriminant version of the RII for all three RI thresholds. Probabilities obtained for the scaled version of the RII (not shown) are generally lower than those shown in Fig. 13. Also shown are the climatological

TABLE 5. As in Table 4, but for the eastern North Pacific sample. The sample sizes for the RI (non-RI samples) for the 25-, 30-, and 35-kt RI thresholds are $N = 255$ (1565), $N = 170$ (1580), and $N = 120$ (1572), respectively.

(a)

Predictor	Units	RI (mean)	RI (std dev)	Non-RI (mean)	Non-RI (std dev)	RI–non-RI (mean)
PER	$m\ s^{-1}$	6.0	4.1	0.4	5.7	**5.6**
D200	$10^{-7}\ s^{-1}$	55.9	29.6	30.7	29.4	**25.2**
SHRD	$m\ s^{-1}$	4.1	1.7	6.4	4.0	**−2.3**
RHLO	%	78.4	4.9	73.4	7.2	**5.0**
POT	$m\ s^{-1}$	49.3	10.1	40.2	14.6	**9.1**
SDBT	°C	11.1	4.6	15.1	6.5	**−4.0**
PX30	%	85.8	13.6	58.7	28.8	**27.1**

(b)

Predictor	Units	RI (mean)	RI (std dev)	Non-RI (mean)	Non-RI (std dev)	RI–non-RI (mean)
PER	$m\ s^{-1}$	6.6	4.0	0.8	5.6	**5.8**
D200	$10^{-7}\ s^{-1}$	59.1	30.6	31.8	29.5	**27.3**
SHRD	$m\ s^{-1}$	3.9	1.5	6.4	3.9	**−2.5**
RHLO	%	78.4	4.8	73.7	7.1	**4.7**
POT	$m\ s^{-1}$	49.2	9.4	41.9	13.8	**7.3**
SDBT	°C	10.5	4.3	15.2	6.5	**−4.7**
PX30	%	87.3	12.8	59.6	28.8	**27.7**

(c)

Predictor	Units	RI (mean)	RI (std dev)	Non-RI (mean)	Non-RI (std dev)	RI–non-RI (mean)
PER	$m\ s^{-1}$	7.4	3.8	1.0	5.5	**6.4**
D200	$10^{-7}\ s^{-1}$	63.2	31.1	32.5	29.5	**30.7**
SHRD	$m\ s^{-1}$	3.8	1.5	6.4	4.0	**−2.6**
RHLO	%	78.6	4.7	73.9	7.0	**4.7**
POT	$m\ s^{-1}$	48.9	9.0	43.0	13.1	**5.9**
SDBT	°C	9.9	4.1	15.2	6.5	**−5.3**
PX30	%	89.6	11	59.6	28.7	**30.0**

RI probabilities of 12.8%, 8.6%, and 6.0% for the 25-, 30-, and 35-kt RI thresholds, respectively. These probabilities are computed from the 1995–2006 eastern North Pacific developmental samples in the same manner as was used for the Atlantic basin. The RI probabilities for the eastern North Pacific basin are generally found to increase for increasing values of R_d (higher quartile value) as well as for decreasing values of the RI threshold. It can be seen that the probabilities for the fourth quartile are 6–10 times as large as climatology.

It is worth noting that the RI probabilities for the eastern North Pacific basin are significantly higher than those obtained for the Atlantic basin (Fig. 10). The reason for this is not obvious. Perhaps the environment in the eastern North Pacific is more predictable or less variable over the scales that are evaluated for each of the RI predictors. Alternatively, perhaps the newly formed eastern North Pacific tropical cyclones are better organized than those in the Atlantic and thus with all others conditions being equal are more likely to undergo RI. Finally, it is possible that the proximity to land of many of the Atlantic basins systems results in lower RI probabilities in that region since systems near land might experience a reduction in overall moisture and an interruption in low-level circulation both of which would tend to reduce the likelihood of undergoing RI.

Figure 14 shows the skill of the eastern North Pacific RII relative to those obtained assuming a climatological rate of RI for each of the three RI thresholds determined utilizing the methodology previously used to compute skill in the Atlantic basin. The skill is shown for both the scaled and discriminant versions of the RII. Similar to the Atlantic basin findings, Fig. 14 shows that the discriminant version of the RII is more skillful than the scaled version for each RI threshold and that the level of skill decreases somewhat as the RI threshold increases.

4. Verification of the RII for independent samples

The results from section 3 show that the RII is skillful relative to forecasts made based upon climatology for both the Atlantic and eastern North Pacific basins for the 1995–2006 developmental sample. In this section, two approaches are employed to verify the RII for an

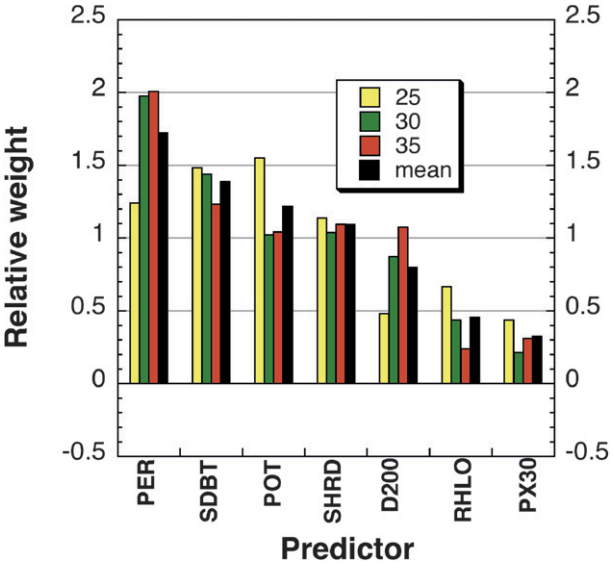

FIG. 12. As in Fig. 9, but for the eastern North Pacific basin.

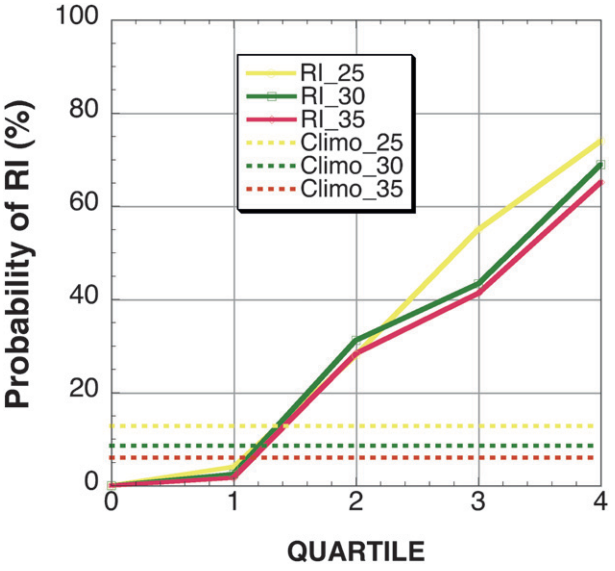

FIG. 13. As in Fig. 10, but for the eastern North Pacific basin.

independent sample to better assess its potential real-time performance. First, a probabilistic verification of the RII forecasts is performed in the same manner used in the previous section. Second, a verification of the RII forecasts in a deterministic form (RI is forecast when the probability is above a specified threshold) is conducted and compared to those of the other operational intensity guidance options.

a. Probabilistic verification

To assess the skill of the RII for an independent sample, the method of cross validation (Wilks 2006) is employed for both the eastern North Pacific and Atlantic basin samples. To accomplish this, the storms from each of the individual years that composed the 12-yr developmental sample (1995–2006) are excluded and the RII is rederived for each RI threshold using only cases from the remaining 11-yr sample. The RII that is derived using data from the 11 yr of developmental data is then run on the cases from the excluded year. This procedure is repeated for each of the individual years that compose the 12 yr Atlantic and eastern North Pacific samples and the results tabulated to get the skill of the RII for the period 1995–2006. It is important to note that the skill obtained by the method of cross validation represents the maximum possible skill of the RII since the observed values of the RI predictors are used when evaluating the RII. Later in this section, a truly independent validation of the index is performed for the two most recent hurricane seasons using forecasted rather than observed RI predictor values.

Figure 15 shows the skill of the scaled and discriminant versions of the RII utilizing the cross-validation technique described above for both the Atlantic and eastern North Pacific basins. The skill of the RII for the developmental samples (Figs. 11 and 14) is also provided. It can be seen that the RII has skill for all three RI thresholds in both basins. However, as expected, the skill is somewhat less than that previously obtained for the developmental sample. The decrease in skill is smaller for the scaled version of the RII compared to the discriminant version. This occurs since only the maximum and minimum values of each predictor are used to derive the scaled version and these typically change very little when a single year is removed from the entire developmental

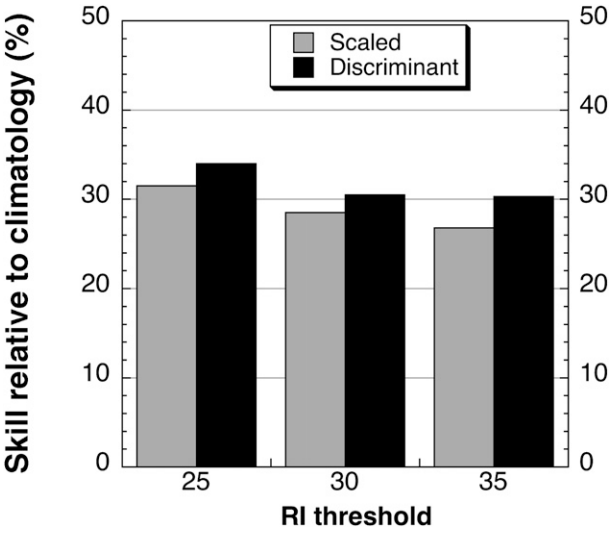

FIG. 14. As in Fig. 11, but for the eastern North Pacific basin. The sample size is 1988.

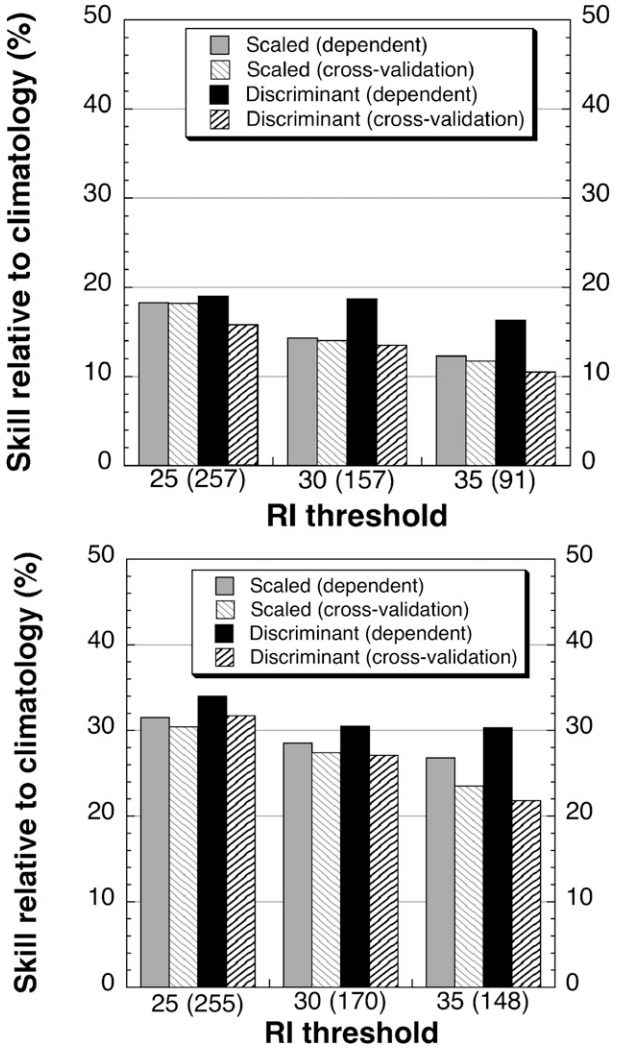

FIG. 15. The skill levels of the (top) Atlantic basin and (bottom) eastern North Pacific basin RIIs for the 1995–2006 dependent and independent cross-validation forecasts. The skill is depicted for the 25-, 30-, and 35-kt RI thresholds for both the scaled and discriminant versions of the RII. The number of RI cases for each RI threshold is shown in parentheses along the x axis. The Atlantic basin sample size is 2140 and the eastern North Pacific sample size is 1988.

sample. In contrast, the W_n values of each RI predictor that are used to compute the RII can change more significantly when an entire year of the developmental sample is removed.

It can be seen that the skill of the scaled version of the RII is slightly higher than the discriminant version in the Atlantic basin, while the skill of both versions is comparable in the eastern North Pacific basin. These findings contrast with the previously described dependent results that showed that the discriminant version of the RII was superior to the scaled version for all of the RI thresholds in each basin. It is anticipated that once the developmental sample size is increased that the cross-validation results will resemble those from the developmental sample.

To simulate the real-time performance of the RII, the index was rerun for all cases from the 2006 and 2007 hurricane seasons. To accomplish this, the RII was first rederived using the developmental data for the period up to but not including the independent years of 2006 and 2007. To illustrate, the developmental data from 1995 to 2005 were used to derive the versions of the RII that were verified for the independent 2006 season forecasts. This was done to simulate the operational performance of the RII since the SHIPS model and RII are rederived prior to each hurricane season in the same manner. The operational storm tracks and NCEP forecast fields that were archived for those two hurricane seasons were then employed to rerun the RII for all of the cases from each season.

Figure 16 shows the skill of the RII relative to climatology for the combined 2006–07 sample. It can be seen that RII exhibited some skill in each basin for all of the RI thresholds, save for the scaled version in the eastern North Pacific for the 35-kt threshold. Also, Fig. 16 shows that the scaled version of the RII is generally more skillful than the discriminant version in the Atlantic basin, while the discriminant RII is the most skillful in the eastern North Pacific. These results are similar to the previously discussed cross-validation results that showed the skill of both versions of the index to be similar. However, they differ from the results obtained previously for the developmental sample that showed the discriminant version of the RII to be superior to the scaled version in each basin. Another noteworthy difference between these results and the dependent results discussed previously is that while the Atlantic independent results show decreasing skill for increasing RI threshold magnitude in agreement with the results in Figs. 11 and 14, the eastern North Pacific basin results show the opposite trend. Both of the above differences between the independent and dependent samples suggest that a larger sample size is required to replicate the results of the developmental sample.

b. Deterministic verification

The aforementioned probabilistic verification showed that the probabilities obtained using the RII are generally skillful compared to those based upon climatology. In this section, the capability of the RII to forecast episodes of RI using a more deterministic approach is evaluated and compared to that of the other operational intensity guidance options. The use of a deterministic approach requires choosing a single probability threshold

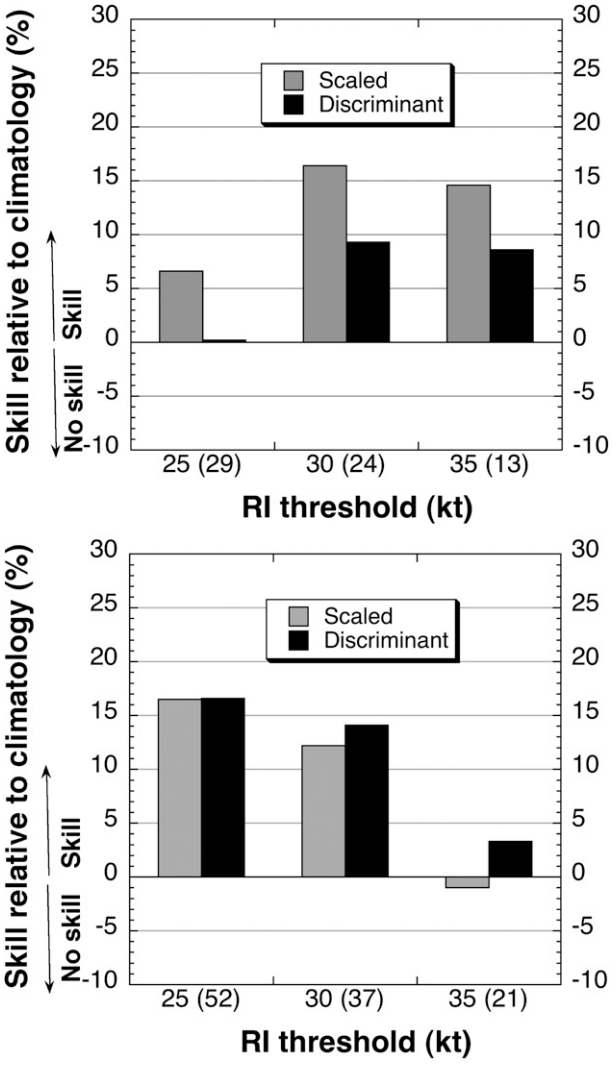

FIG. 16. The skill of the scaled and discriminant versions of the RII for the independent 2006 and 2007 (top) Atlantic ($N = 263$) and (bottom) eastern North Pacific ($N = 448$) rerun forecasts. The number of RI cases for each RI threshold is shown in parentheses along the x axis.

to forecast whether or not RI will occur over the succeeding 24 h. As described in Wilks (2006), a single value of the discriminant function (and hence a single probability since these values are converted to probabilities in this study) can be computed that separates the developmental sample into two groups. This value can then be used as a cutoff such that cases that have discriminant values that equal or exceed it are placed into one group (RI group in this study) while those below it are placed into another (non-RI group). Although the above technique is adequate for most samples, Wilks (1995) notes that it may not work that well for such rare events as RI. In such instances, Wilks suggests that it may be preferable to choose the discriminant cutoff value so that more cases fall into the group with the highest likelihood of membership (e.g., non-RI group in this study).

Thus, in the current study the dividing point that is used to determine whether to assign a case to the RI or non-RI group is the value of the discriminant function that matches the climatological probability of false detection (POFD) of the dependent sample. As is described in Wilks (2006), the POFD (also known as the false alarm rate) is the ratio of the number of times that an event is forecast to occur but does not, divided by the total number of times that an event does not occur. For example, if RI is forecast twice and does not occur a total of 10 times, then the POFD is 0.2 ($^2/_{10}$). The climatological POFD is used since it is a relatively conservative quantity that sensitivity tests showed yielded higher discriminant cutoff values (i.e., RI probabilities) and hence more non-RI cases, as suggested in Wilks (1995).

For each RI threshold, the POFD can be estimated both for climatology, as well as for the dependent samples. The climatological POFD can be approximated by the climatological probability of RI divided by one plus the climatological probability of RI for each RI threshold. The POFD of the dependent samples can also be approximated for each of the quartiles. To accomplish this it is assumed that RI is forecast for any case with a discriminant value (R_d) that exceeds the upper limit of each of the four quartiles; and conversely is not forecast for cases with discriminant values below that value. For example, assume first that there are 15 cases with R_d values greater than the first quartile threshold and that 10 of those are non-RI cases while 5 are RI cases. Also, assume that there are 30 non-RI cases with discriminant values lower than the threshold of the first quartile. Thus, the total number of non-RI cases observed is 40 (10 + 30). Consequently, the POFD would be 0.25 [(10 RI cases forecasted but not observed)/(40 non-RI cases observed)].

The above procedure is repeated to estimate the POFD between each of the four quartiles such that three POFD values are determined for each RI threshold. These POFD values are then linearly interpolated to determine the value of the discriminant function where the POFD computed from the developmental sample matches that of climatology. This procedure is repeated for each of the three RI thresholds for both the Atlantic and eastern North Pacific basin to find the discriminant (and hence probability) cutoff thresholds for both the 1995–2005 and 1995–2006 developmental samples.

Table 6 shows the probability of RI cutoff thresholds for the Atlantic and eastern North Pacific basins for the 25-, 30-, and 35-kt versions of the RII. The 1995–2005 RI cutoff thresholds are used to make forecasts of RI for the independent 2006 sample, while the 1995–2006 cutoff

TABLE 6. RII probability thresholds (%) used to forecast RI for the independent 2006 and 2007 (top) Atlantic and (bottom) eastern North Pacific basin samples.

Atlantic		
RI threshold	2006	2007
25	23.6	29.8
30	20.9	20.3
35	20.0	20.6
Eastern North Pacific		
RI threshold	2006	2007
25	32.5	35.2
30	33.6	30.6
35	26.7	28.3

thresholds are used to make forecasts for the independent 2007 sample. To accomplish this, the previously computed probability of RI values of the 2006 (2007) independent rerun forecasts are compared to the corresponding 1995–2005 (1995–2006) RI cutoff probability thresholds for each of the three RI thresholds. Rapid intensification is forecast if the probability of RI computed for a given RI threshold equals or exceeds the probability of RI cutoff thresholds in Table 6.

The ability of the other operational intensity guidance options that were available for both the 2006 and 2007 Hurricane seasons to predict RI is also evaluated for these same cases. For this study, RI is declared forecast by either a model or the NHC if the 24-h forecast intensity change exceeds the corresponding RI threshold. For example, if the forecasted 24-h intensity change of a model or NHC is 26 kt, then RI is declared forecast for the 25-kt threshold but not the 30- or 35-kt RI thresholds. The observed 24-h intensity changes determined from the NHC HURDAT database and the operational 24-h forecasted intensity changes obtained from the Automated Tropical Cyclone Forecast (ATCF) system (Sampson and Schrader 2000) are employed to assess whether or not a model or the NHC correctly forecast RI for each 24-h forecast period.

Figure 17 shows the verification of the deterministic RI forecasts for the Atlantic and eastern North Pacific basins for the 2006 and 2007 hurricane seasons. To be consistent with the methodology used to develop the revised RII, only cases that remained both over water and were classified by NHC as tropical or subtropical for the entire 24-h period are verified. The results are shown for a homogeneous sample of forecasts made using the RII, the decay version of the SHIPS model (DSHP), the Geophysical Fluid Dynamic Laboratory model (GFDL) (Kurihara et al. 1998), the Statistical Hurricane intensity Forecast Model (SHF5) (Knaff et al. 2003), and the NHC official forecast (OFCL). The eastern North Pacific samples sizes differ from those in Fig. 16, since an RI case was only used if forecasts from all the operational intensity forecast guidance schemes were available and this was not true for some of the eastern North Pacific RI cases due mainly to the absence of some GFDL model forecasts.

The three metrics used to evaluate the skill of the RI forecasts are the probability of detection (POD), the false alarm ratio (FAR), and the Peirce skill score (PSS). The POD (Wilks 2006) is the percentage of RI cases that are correctly identified. For example, if a model correctly forecasts RI 5 out of the 10 times that RI is observed, then the probability of detection is 50%. The FAR is the number of times that RI is forecasted but does not occur divided by the total number of times RI is forecast. Thus, if a model forecasts RI on 10 occasions but RI is observed for only 2 of those cases, then the false alarm ratio is 80% (8/10). The PSS is used to evaluate the overall skill of contingency type forecasts and is particularly helpful for evaluating forecasts of such rare events as RI (Wilks 2006). The PSS is equivalent to POD–POFD and is 1 for a perfect forecast and 0 for random or constant forecasts. Forecasts that are worse than random forecasts receive negative scores.

It can be seen that for the 2006 and 2007 Atlantic basin samples, the POD of the RII is higher than the other operational intensity guidance options for each RI threshold. Although the FAR of the RII is also fairly high for all three RI thresholds, they are generally within the envelope of those obtained from the other intensity guidance choices. Specifically, the OFCL forecasts have the lowest FAR for all three RI thresholds, while the GFDL model had the highest values for the 25- and 30-kt thresholds, and the RII the highest for the 35-kt RI threshold. It is important to note that no FAR is provided for models that did not have forecasts of RI for a given RI threshold since by definition it is an undefined quantity. For example, SHF5 had no forecasts of RI in the Atlantic basin for any of the RI thresholds and thus no values of FAR appear for this model. Similarly, the DSHP model had no forecasts of RI for the 30- and 35-kt thresholds and the GFDL had none for the 35-kt RI threshold. Thus, no FAR is shown for these RI thresholds for either DSHP or GFDL.

It is interesting to note that both the statistical (DSHP and RII) and dynamical (GFDL) intensity model guidance exhibit low to moderate POD and rather high FAR. Elsberry et al. (2007) found similar trends during their study of the accuracy of operational intensity guidance during the 2003 and 2004 hurricane seasons. While the reasons for these findings are unclear, perhaps they are due, in part, to the lack of detailed inner-core

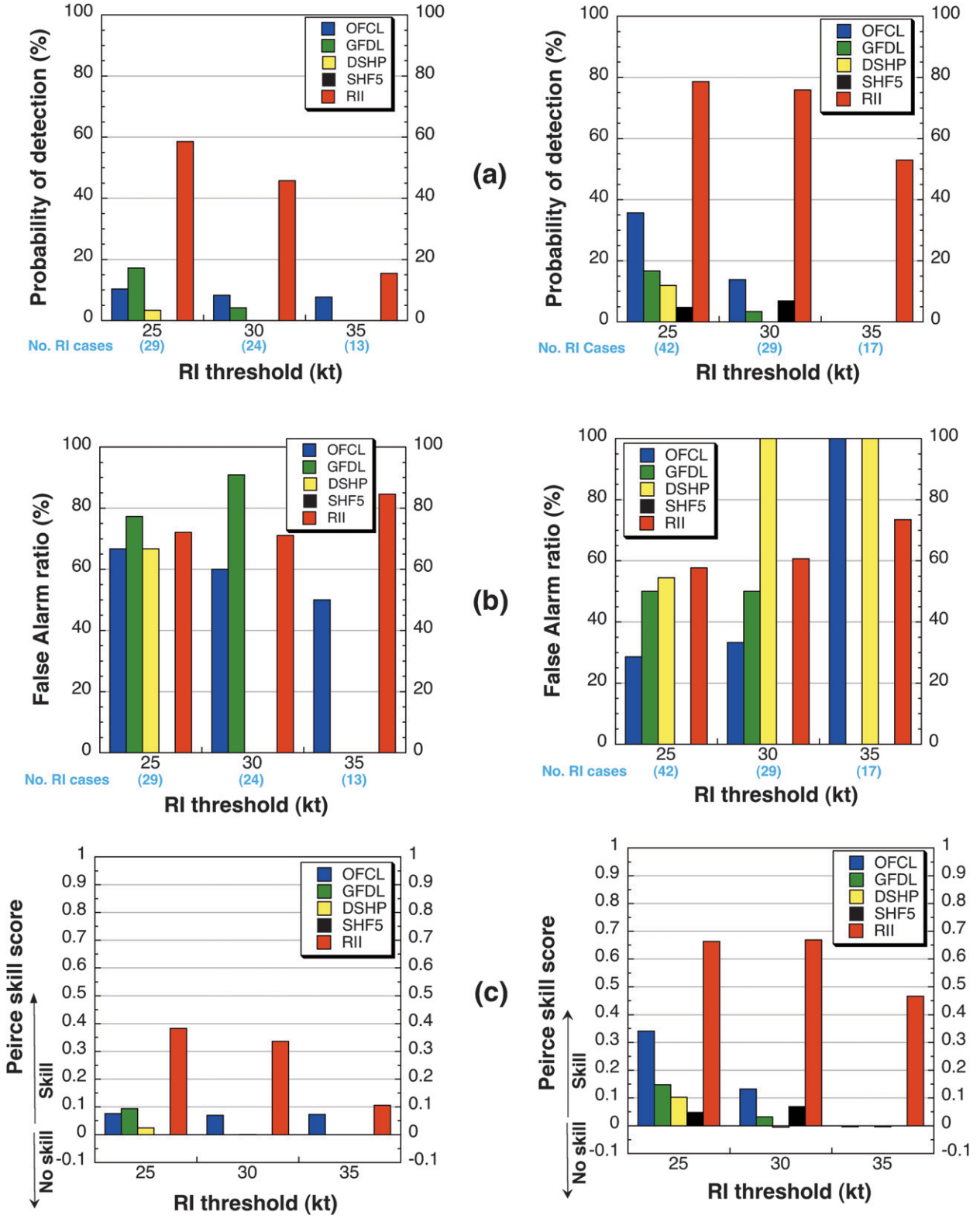

FIG. 17. (a) PODs, (b) FARs, and (c) PSSs of the 2006 and 2007 (left) Atlantic and (right) eastern North Pacific deterministic RI forecasts. Results are shown for GFDL, DSHP, SHF5, RII, and OFCL forecasts for the 25-, 30-, and 35-kt RI thresholds. The number of RI cases for each RI threshold is provided in parentheses (light blue) along the *x* axis for each RI threshold.

structure information in both the dynamical and statistical model guidance options.

Despite the rather high FAR, the RII is skillful (positive values of PSS) for all three RI thresholds, as is the OFCL forecast. The GFDL and DSHP forecasts also have some skill for the 25-kt RI threshold but not the 30- and 35-kt thresholds. It should be noted that only a 25-kt version of the RII was provided to NHC in real time during the 2006 and 2007 hurricanes seasons and thus the skill levels shown for the 30- and 35-kt OFCL RI forecasts are likely to be lower-bound estimates.

The 2006 and 2007 eastern North Pacific RI verification results show that the POD of the RII is higher than the other intensity guidance options, while the FAR of the RII is within the range of values obtained for the other intensity guidance options for all three RI thresholds. It can be seen that the OFCL forecasts had the lowest FAR for the 25- and 30-kt RI thresholds and the RII had the lowest for the 35-kt threshold. It is interesting to note that the POD (FAR) of the eastern North Pacific RII is higher (lower) than the corresponding values obtained for the Atlantic basin. A similar trend of higher POD and lower FAR in the eastern North Pacific compared to that in the Atlantic is found for the OFCL forecasts for the 25- and 30-kt RI thresholds but not for the 35-kt threshold.

The PSSs for the RII are positive for all three RI thresholds indicating that the RII had skill for the independent eastern North Pacific sample. The OFCL, GFDL, and SHF5 forecasts were also skillful by this measure for the 25- and 30-kt RI threshold, but not the 35-kt RI threshold. The DSHP forecasts were only skillful for the 25-kt RI threshold. The finding of higher skill for the RII in predicting RI in the eastern North Pacific basin than in the Atlantic basin suggests that the importance of the large-scale environment on RI may be greater in the eastern North Pacific, since the large-scale predictors used in the RII are nearly identical in both basins. Thus, obtaining information about a tropical cyclone's inner-core structure may be more crucial for predicting RI in the Atlantic than in the eastern North Pacific basin.

5. Conclusions

A revised rapid intensity index (RII) was developed for the Atlantic and eastern North Pacific basins utilizing linear discriminant analysis. The RII employed large-scale predictors from the Statistical Hurricane intensity Prediction Scheme (SHIPS) to estimate the probability of RI over the succeeding 24 h. Separate versions of the RII were developed for the 25-, 30-, and 35-kt RI thresholds, which represent the 90th (88th), 94th (92nd), and 97th (94th) percentiles of 24-h overwater intensity changes of tropical and subtropical cyclones in the Atlantic (eastern North Pacific) basins from 1989 to 2006, respectively. The revised RII was declared operational by the TPC/NHC prior to the 2008 hurricane season.

An analysis of the climatology of RI cases was also performed. It was shown that the Atlantic RI cases tended to occur over a fairly widespread region. In contrast, the eastern North Pacific RI cases tended to be more tightly clustered and were mainly found between 10°–20°N and 95°–140°W. Although the majority of the RI cases developed in September in both basins, the Atlantic basin had about twice as many RI occurrences in the latter months of the hurricane season (October and November) compared to the earlier months (June and July) whereas in the eastern North Pacific the earlier months had about twice as many RI occurrences as the latter months. In both basins, systems that were initially of weak tropical storm intensity contributed the highest percentage of RI cases for the 25- and 30-kt RI thresholds, while those that were of strong tropical storm or weak hurricane intensity made up the highest percentage of systems that satisfied the 35-kt threshold.

The relative importance of the individual predictors to the RII was shown to vary both within and between both basins. Specifically, the kinematic predictors (upper-level divergence and vertical wind shear) and the previous 12-h intensity change were found to have the highest weights for the Atlantic basin. In contrast, the previous 12-h change in the intensity, the symmetry of inner-core convection, and the difference in a system's current and maximum potential intensity were weighted highest in the eastern North Pacific basin.

A verification of independent probabilistic forecasts from the 2006 and 2007 hurricane seasons showed that the RII was generally skillful for both the Atlantic and eastern North Pacific basins. Moreover, when utilized in a deterministic manner, the RII performed well relative to the other operational intensity guidance options in terms of the probability of detection (POD) and false alarm ratio (FAR) of RI events in both basins. Specifically the POD for the RII ranged from 15% to 59% (53% to 73%) while the FAR ranged from 71% to 85% (53% to 79%) in the Atlantic (eastern North Pacific) basins, respectively. Although it is not clear why the RII exhibits substantially more skill for the eastern North Pacific basin, it is possible that the large-scale environment may play a more prominent role in the RI process in that basin.

Finally, the modest POD and relatively high FAR of the RII and other intensity guidance options demonstrate the difficulty of predicting RI, particularly in the

Atlantic basin. Since the RII uses mainly large-scale predictors, these results suggest that more detailed inner-core information is likely required to improve the skill of the RII and perhaps other intensity models. The use of more detailed inner-core information in the RII will be the subject of future research.

Acknowledgments. We wish to thank Paul Leighton of HRD and Nicholas Carrasco (University of Miami–HRD) for their valuable assistance in writing the computer code that was used to verify the deterministic RI forecasts and the TPC/NHC hurricane specialists for their helpful feedback and suggestions during the course of this study. Robert DeMaria of Colorado State University wrote the code to plot the tracks of the RI cases. This manuscript was greatly improved by the helpful suggestions of Dr. Frank Marks and Jason Dunion of HRD, as well as the thoughtful reviews of Michael Split and two anonymous reviewers. This research was supported, in part, by grants from the NOAA Joint Hurricane Testbed (JHT). The views, opinions, and findings in this report are those of the authors and should not be construed as an official NOAA or U. S. government position, policy, or decision.

REFERENCES

Bosart, L. F., C. S. Velden, W. E. Bracken, J. Molinari, and P. G. Black, 2000: Environmental influences on the rapid intensification of Hurricane Opal (1995) over the Gulf of Mexico. *Mon. Wea. Rev.,* **128,** 322–352.

Cione, J. J., and E. W. Uhlhorn, 2003: Sea surface temperature variability in hurricanes: Implications with respect to intensity change. *Mon. Wea. Rev.,* **131,** 1783–1796.

——, J. Kaplan, C. Gentemann, and M. DeMaria, cited 2009: Developing an inner-core SST cooling algorithm for SHIPS. National Hurricane Center. [Available online at http://www.nhc.noaa.gov/jht/03-05_proj.shtml.]

DeMaria, M., and J. Kaplan, 1994: Sea surface temperature and the maximum intensity of Atlantic tropical cyclones. *J. Climate,* **7,** 1324–1334.

——, J. A. Knaff, and B. H. Connell, 2001: A tropical cyclone genesis parameter for the tropical Atlantic. *Wea. Forecasting,* **16,** 219–233.

——, M. Mainelli, L. K. Shay, J. A. Knaff, and J. Kaplan, 2005: Further improvements to the Statistical Hurricane Intensity Prediction Scheme (SHIPS). *Wea. Forecasting,* **14,** 1093–1108.

——, J. A. Knaff, and C. Sampson, 2007: Evaluation of long-term trends in tropical cyclone intensity forecasts. *Meteor. Atmos. Phys.,* **97,** 19–28.

Dowdy, S., and S. Wearden, 1991: *Statistics for Research*. 2nd ed. Wiley-Interscience, 555 pp.

Dunion, J. P., and C. S. Velden, 2004: The impact of the Saharan air layer on Atlantic tropical cyclone activity. *Bull. Amer. Meteor. Soc.,* **85,** 353–365.

——, and C. S. Marron, 2008: A reexamination of the Jordan mean tropical sounding based on awareness of the Saharan air layer: Results from 2002. *J. Climate,* **21,** 5242–5253.

Eastin, M., W. M. Gray, and P. G. Black, 2005a: Buoyancy of convective vertical motions in the inner core of intense hurricanes. Part I: General statistics. *Mon. Wea. Rev.,* **133,** 188–208.

——, ——, and ——, 2005b: Buoyancy of convective vertical motions in the inner core of intense hurricanes. Part II: Case studies. *Mon. Wea. Rev.,* **133,** 209–227.

Elsberry, R., T. D. B. Lambert, and M. A. Boothe, 2007: Accuracy of Atlantic and eastern North Pacific tropical cyclone intensity forecast guidance. *Wea. Forecasting,* **22,** 747–762.

Frank, W. M., and E. A. Ritchie, 2001: Effects of vertical wind shear on the intensity and structure of numerically simulated hurricanes. *Mon. Wea. Rev.,* **129,** 2249–2269.

Hanley, D., J. Molinari, and D. Keyser, 2001: A composite study of the interactions between tropical cyclones and upper-tropospheric troughs. *Mon. Wea. Rev.,* **129,** 2570–2584.

Gray, W. M., 1968: Global view of the origin of tropical disturbances and storms. *Mon. Wea. Rev.,* **96,** 669–700.

Hong, X., S. W. Chang, S. Raman, L. K. Shay, and R. Hodur, 2000: The interaction between Hurricane Opal (1995) and a warm core ring in the Gulf of Mexico. *Mon. Wea. Rev.,* **128,** 1347–1365.

Jarvinen, B. R., C. J. Neumann, and M. A. S. Davis, 1984: A tropical cyclone data tape for the North Atlantic basin, 1886–1983: Contents, limitations, and uses. NOAA Tech. Memo. NWS NHC 22, Miami, FL, 21 pp. [Available from National Technical Information Service, 5285 Port Royal Rd., Springfield, VA 22151.]

Kaplan, J., and M. DeMaria, 2003: Large-scale characteristics of rapidly intensifying tropical cyclones in the North Atlantic basin. *Wea. Forecasting,* **18,** 1093–1108.

Knaff, J. A., M. DeMaria, J. Kaplan, C. R. Sampson, and J. M. Gross, 2003: Statistical 5-Day tropical cyclone intensity forecasts derived from climatology and persistence. *Wea. Forecasting,* **18,** 80–92.

——, ——, and ——, cited 2009: Improved statistical intensity forecast models. National Hurricane Center. [Available online at http://www.nhc.noaa.gov/jht/05-07_proj.shtml.]

Kossin, J., and W. H. Schubert, 2001: Mesovortices, polygonal flow patterns, and rapid pressure falls in hurricane-like vortices. *J. Atmos. Sci.,* **58,** 1079–1090.

Kurihara, Y., R. E. Tuleya, and M. A. Bender, 1998: The GFDL Hurricane Prediction System and its performance in the 1995 hurricane season. *Mon. Wea. Rev.,* **126,** 1306–1322.

Levitus, S., 1982: *Climatological Atlas of the World Ocean*. NOAA Prof. Paper 13, 173 pp. [Available from U.S. Government Printing Office, Washington, DC 20402.]

Mainelli, M., M. DeMaria, L. K. Shay, and G. Goni, 2008: Application of oceanic heat content estimation to operational forecasting of recent Atlantic category 5 hurricanes. *Wea. Forecasting,* **23,** 3–16.

Molinari, J., and D. Vollaro, 1990: External influences on hurricane intensity. Part II: Vertical structure and response of the hurricane vortex. *J. Atmos. Sci.,* **47,** 1902–1918.

Mueller, K. J., M. DeMaria, J. A. Knaff, J. P. Kossin, and T. H. Vonder Haar, 2006: Objective estimation of tropical cyclone wind structure from infrared satellite data. *Wea. Forecasting,* **21,** 990–1005.

NHC, cited 2008: Joint Hurricane Testbed (JHT) opportunities for transfer of research and technology into tropical cyclone analysis and forecast operations. [Available online at http://www.nhc.noaa.gov/jht/index.shtml.]

Nolan, D. S., and L. D. Grasso, 2003: Three-dimensional perturbations to balanced, hurricane-like vortices. Part II: Symmetric response and nonlinear simulations. *J. Atmos. Sci.,* **60,** 2717–2745.

Reynolds, R. W., and T. M. Smith, 1993: An improved real-time global sea surface temperature analysis. *J. Climate,* **6,** 114–119.

Sampson, C. R., and A. J. Schrader, 2000: The Automated Tropical Cyclone Forecasting System (version 3.2). *Bull. Amer. Meteor. Soc.,* **81,** 1231–1240.

Schubert, W. H., and J. J. Hack, 1982: Inertial stability and tropical cyclone development. *J. Atmos. Sci.,* **39,** 1687–1697.

Shay, L. K., G. J. Goni, and P. G. Black, 2000: Effects of a warm oceanic feature on Hurricane Opal. *Mon. Wea. Rev.,* **128,** 1366–1383.

Sitkowski, M., and G. M. Barnes, 2009: Low-level thermodynamic, kinematic, and reflectivity fields of Hurricane Guillermo (1997) during rapid intensification. *Mon. Wea. Rev.,* **137,** 645–663.

Wilks, D. S., 1995: *Statistical Methods in the Atmospheric Sciences: An Introduction*. Academic Press, 467 pp.

——, 2006: *Statistical Methods in the Atmospheric Sciences*. 2nd ed. Academic Press, 627 pp.

Willoughby, H. E., J. A. Clos, and M. G. Shoreibah, 1982: Concentric eyewalls, secondary wind maxima, and the evolution of the hurricane vortex. *J. Atmos. Sci.,* **39,** 395–411.